Microplasma Array Serving as Photonic Crystals and Plasmon Chains*)

Osamu SAKAI, Teruki NAITO and Kunihide TACHIBANA

Department of Electronic Science and Engineering, Kyoto University, Kyoto 615-8510, Japan

(Received 9 September 2008 / Accepted 7 March 2009)

An array of microplasmas with sizes ranging from a millimeter to a micrometer, has potential for novel and promising electromagnetic-wave media, especially when the wave frequency is below the electron plasma frequency. Photonic crystals or band-gap materials composed of microplasmas have unique properties arising from their loss term, and they can become band-pass filters instead of the band-stop filters usually observed in photonic crystals of dielectrics. Such behavior is well understood using the dispersion relation in a three-dimensional space of frequency and complex wavenumber with real and imaginary parts. Another functional array is a simple one-dimensional (1D) array; it can conduct microwaves for a wide frequency range below the electron plasma frequency. The propagating modes are similar to the coupling of localized surface plasmon polaritons observed along a metallic nanoparticle chain in the photon range; however a 1D microplasma array features differ from those of a metallic sphere array, leading to a dynamic wide-band waveguide.

Keywords: microplasma, electromagnetic waves, photonic crystal, surface wave, localized surface plasmon polariton

DOI: 10.1585/pfr.4.052

1. Introduction

Electromagnetic waves propagating in a large plasma have been explored in plasma physics for wide application to control fusion plasmas and to understand phenomena in the ionosphere [1, 2]. In most cases wave propagation has been investigated implicitly in the region where the plasma size is larger than the wavelength of electromagnetic waves. Plasma production for material processing has been also in similar regimes, where radiofrequency waves and microwaves with their wavelength less than the characteristic length of the device are the sources of power consumption or are simply coupled to a plasma capacitively or inductively.

The present report investigates wave propagation where the wavelength is comparable to the characteristic length of a given periodic structure. Another important aspect of our study is the spatial design of plasma discontinuities and periodicities, around which electromagnetic waves transmit and reflect due to different refractive indexes in both cases, and sometimes propagate as surface wave modes. Furthermore, since available plasmas in gas discharges are collisional, electron elastic collisions induce an imaginary part of the wavenumber. To study such matters, this report focuses on uses of microplasmas with size ranging from a millimeter to a micrometer and electron densities n_e ranges from $10^{12}\,\mathrm{cm}^{-3}$ to $10^{16}\,\mathrm{cm}^{-3}$.

Periodic structure in the range of the wavelength of electromagnetic waves has been well investigated as photonic crystals in photonics [3, 4], in which dielectrics are arranged periodically in two- or three-dimensional (2D or 3D) space. Band gaps and other prominent features have been observed so far. If we use microplasmas as components of photonic crystals, the time-varying and frequency-dependent dielectric constant in plasmas is expected to add novel functions to photonic crystals. This has been proposed theoretically [5–7] and verified experimentally [8–12]. In addition, the effects of the imaginary part of the wavenumber, which are outstanding below the electron plasma frequency ω_{pe}, alter the functions of these band-gap materials significantly [13, 14], which will be explained in this report specifically in Secs. 2 and 3 below.

Another interesting phenomenon of periodic structures in the photon range is a metallic-nanoparticle chain yielding a photon waveguide by coupled localized surface plasmons [15–17]. A similar function for conduction of electromagnetic waves in the microwave range is possible along a microplasma chain below ω_{pe}, based on the suggestions in the previous studies about surface waves on plasmas [18–24]; we reported such phenomena briefly [14]. This phenomenon is also studied in more detail in this manuscript in Secs. 2 and 3 below.

In Sec. 4, we discuss these two functional structures. We point out differences plasma "plasmon" chains and ordinary metallic-nanoparticle chains; aside from the difference in frequency range, their physical properties will be compared. Also we describe the emerging conditions of

author's e-mail: osakai@kuee.kyoto-u.ac.jp

*) This article is based on the invided talk at the 14th International Congress on Plasma Physics (ICPP2008).

band-gap materials and plasmon chains in a microplasma array; this discussion will clarify the requirements for future applications to high-frequency devices using these two structures.

2. Dispersion Relations of Microplasma Array

2.1 Band gap in a complex wavenumber plane

Figure 1 shows the dispersion relation of 2D wave propagation in a 2D microplasma array; in solid physics, it is called a band diagram, and the wavenumber is chosen as a real number. This band diagram was derived using the modified plane-wave expansion method [10], assuming that microplasmas with an electron density of 4×10^{13} cm^{-3} and diameter of 1.0 mm were arranged in a square lattice of lattice constant $a = 2.5$ mm, surrounded by a dielectric with permittivity of 3.0. The electron elastic collision frequency ν_m was set to $0.5\omega_{pe}$. When the electromagnetic wave frequency $\omega/2\pi$ was above $\omega_{pe}/2\pi$, features similar to those in band diagrams in a dielectric photonic crystal were observed. Below ω_{pe}, flat bands with very low group velocity were present throughout the frequency, and a branch along the light line went across them. A band gap in the Γ-X direction was found around $\omega a/2\pi c = 0.3$ along this branch. This band gap is well below ω_{pe}, where the permittivity is less than zero, and an additional property may be present that does not occur in typical dielectric photonic crystals.

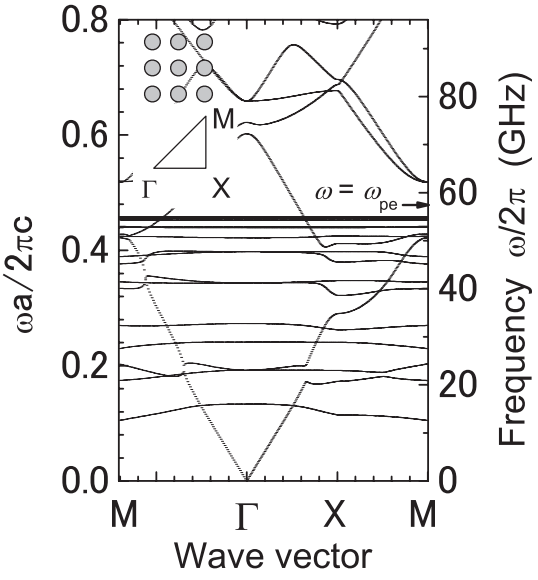

Fig. 1 Dispersion relation (or band diagram) of microplasma array calculated by modified plane-expansion method. Microplasma has a diameter of 1.0 mm with lattice constant of square lattice 2.5 mm. The shape of the profile of electron density of 4×10^{13} cm^{-3} resembles that in the slab case, and the electron elastic collision frequency is set to be $0.5\omega_{pe}$.

In a general collisional plasma, the loss term of electromagnetic waves arising from electron elastic collisions becomes large below ω_{pe}. Such a tendency is displayed in Fig. 2, where the imaginary part of the wavenumber k_i as well as the real part k_r in a bulk plasma is shown in a 3D $\omega - k_r - k_i$ space. We assume that the permittivity ε is in the Drude model, as

$$\varepsilon = 1 - \frac{\omega_{pe}^2}{\omega^2}\frac{1}{1 - j(\nu_m/\omega)}. \quad (1)$$

To derive the dispersion relation in Fig. 2, $\omega_{pe}/2\pi$ is set to 57 GHz, and $\nu_m = 0.5\omega_{pe}$. k_r is not zero even when $\omega < \omega_{pe}$, although the real part of ε is negative where $\omega^2 < \omega_{pe}^2 + \nu_m^2$. k_i is large when $\omega < \omega_{pe}$, and k_r and k_i are not coupled via a simple function. The resultant trajectory on the $k_r - k_i$ plane is complicated, and so the propagation constant ($\gamma = \alpha - j\beta$) is very distinctive in a plasma, unlike in other solid materials.

When we consider such effects resulting from the complicated k_r and k_i relationship, other underlying properties of lossy band gap materials can be noted. In Fig. 3, we redrew the part of the band diagram in the Γ-X direction in Fig. 1 in a similar manner to Fig. 2; not only $\omega - k_r$ but also $\omega - k_i$ was plotted using the relation $\omega_i = -v_g k_i$ [25], where $v_g = d\omega/dk$ and ω_i is the imaginary part of the wave angular frequency derived by the modified plane-wave expansion method. We also note that a number of the flat bands shown in Fig. 1 were removed, and we concentrated on the branch along the light line.

In the $\omega - k_r$ plane in Fig. 3, a band gap was clearly observed from $\omega a/2\pi c = 0.29$ to 0.32, and the dispersion relation was divided into upper and lower bands. In the lower band, there was a gap from $\omega a/2\pi c = 0.17$ to 0.21 arising from the crossing of one flat band, but k_r and k_i were continuous on both sides of the gap. This fact indicates that this is a simple frequency band gap caused by deformation of the flat-band crossing.

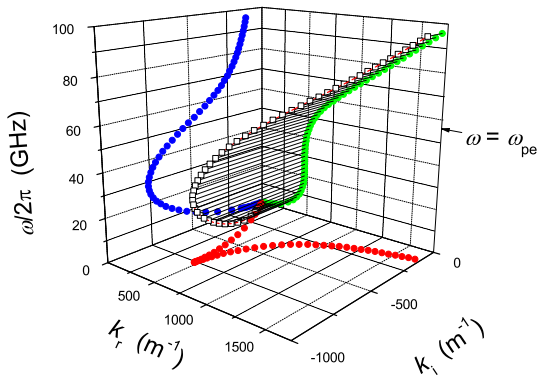

Fig. 2 Dispersion relation of an infinite non-magnetized plasma in 3D space with 3 axes of real and imaginary wavenumber and frequency. Electron density is 4×10^{13} cm^{-3}, and the electron elastic collision frequency is set $0.5\omega_{pe}$.

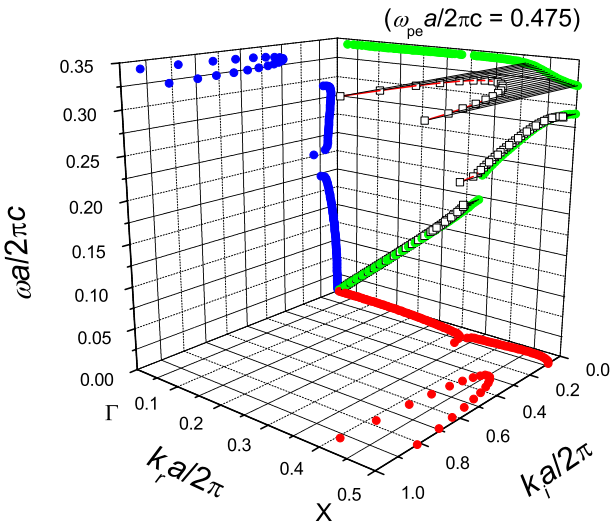

Fig. 3 Dispersion relation (or band diagram) of microplasma array in 3D space with parameters similar to those in Fig. 1. Data points of k_i at $k_i a/2\pi > 1.0$ are out of range in this figure.

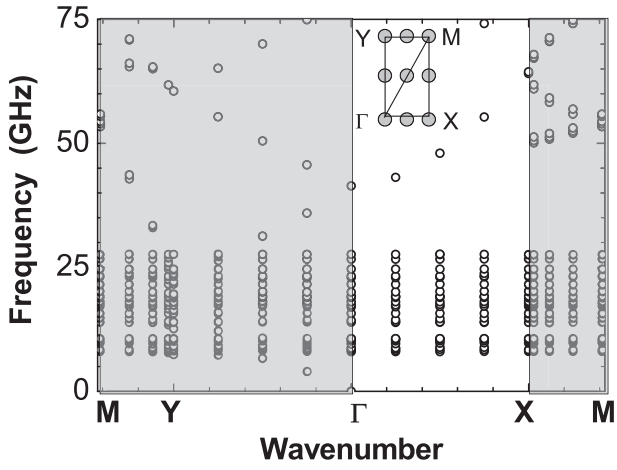

Fig. 4 Dispersion relation (or band diagram) of microplasma array determined by direct calculation of the wave equation with complex electric field. Microplasma has a diameter of 1.0 mm with lattice constants of rectangular lattice 3.0×7.5 mm. The profile of electron density has a peak value of 1×10^{13} cm^{-3}; its shape resembles that of J_0 with zero at the boundary.

However, the band gap from $\omega a/2\pi c = 0.29$ to 0.32 yielded very large differences between the upper and lower bands. Although k_r was equal on both sides at $\omega a/2\pi c = 0.29$ and 0.32, k_i of the upper band was one order of magnitude larger than that of the lower band. The trajectory on the $k_r - k_i$ plane clarifies that these two bands had completely different properties. This is mainly attributed to different wave-field profiles in one lattice [12]. On the upper band, wave fields concentrate on the plasma region where ε is relatively small, but on the lower band, wave fields are localized outside the plasma region where ε is relatively large. If a band gap is located above $\omega_{pe}/2\pi$, the differences in the field profile changes only the matching condition between inside and outside the array regions, and the band gap shows the features of a band-stop filter [11]. On the other hand, if a band gap is located below $\omega_{pe}/2\pi$, the field profile in the periodic structure strongly affects attenuation of the propagating waves by electron elastic collisions [14]. The experimental observation of this band gap will be described in Sec. 3.1.

2.2 Coupling of localized surface waves

As shown in Fig. 1, a number of flat bands are present below $\omega_{pe}/2\pi$, and they are composed of coupled modes of localized surface waves; Ito and Sakoda discussed the coupling conditions in the case of localized surface plasmons (LSPs) on a metal sphere in the photon range [26]. Here we show similar wave propagation by coupling of the localized surface modes, and the outstanding features in the case of plasmas are addressed.

Figure 4 shows the dispersion relation of 2D propagation in a rectangular lattice. This band diagram was derived using the direct solution of the wave equation using complex electric fields [10], and here we assumed that microplasmas with n_e of 1×10^{13} cm^{-3} and diameter of 1.5 mm were arranged in a rectangular lattice of lattice constants $a_x = 3.0$ mm and $a_y = 7.5$ mm, surrounded by free space. Electron elastic collisions were neglected in this calculation for simplicity, and an electron-density profile consisting of a Bessel function of the first kind of the 0th order $J_0(Ar)$ was assumed, where r is the position from the center of the circular cross section of a microplasma, and constant A was set to fulfill the boundary condition with density $n_e = 0$ on its edge. The peak density was set to 1×10^{13} cm^{-3}, which was also the value in the case of the slab density profile with constant n_e in Fig. 5. When we investigate wave propagation along a microplasma "chain," the partial dispersion relation in the Γ-X direction is considered.

At frequencies above $\omega_{pe}/2\pi$ (~28 GHz), propagation in equivalent dielectric poles was observed. At lower frequencies, multiple flat bands with very low group velocity were present, similar to those in Fig. 1; this supports the existence of LSP-like modes, which will be verified later in Fig. 5. Because the bands are almost flat in the $\omega - k$ diagram, they can match various wave modes with different space impedance, which is expressed in the gradient of the $\omega - k$ plot.

In the upper part of Fig. 5, profiles in the slab case exhibit similar features to those of LSPs around a metal sphere [27]; electric fields are concentrated on the surface of the sphere, and the azimuthal mode number of the standing waves l around the sphere increases from $l = 1$ to 4 as the frequency increases. On the other hand, from the knowledge of metal optics, LSPs on the metal sphere are

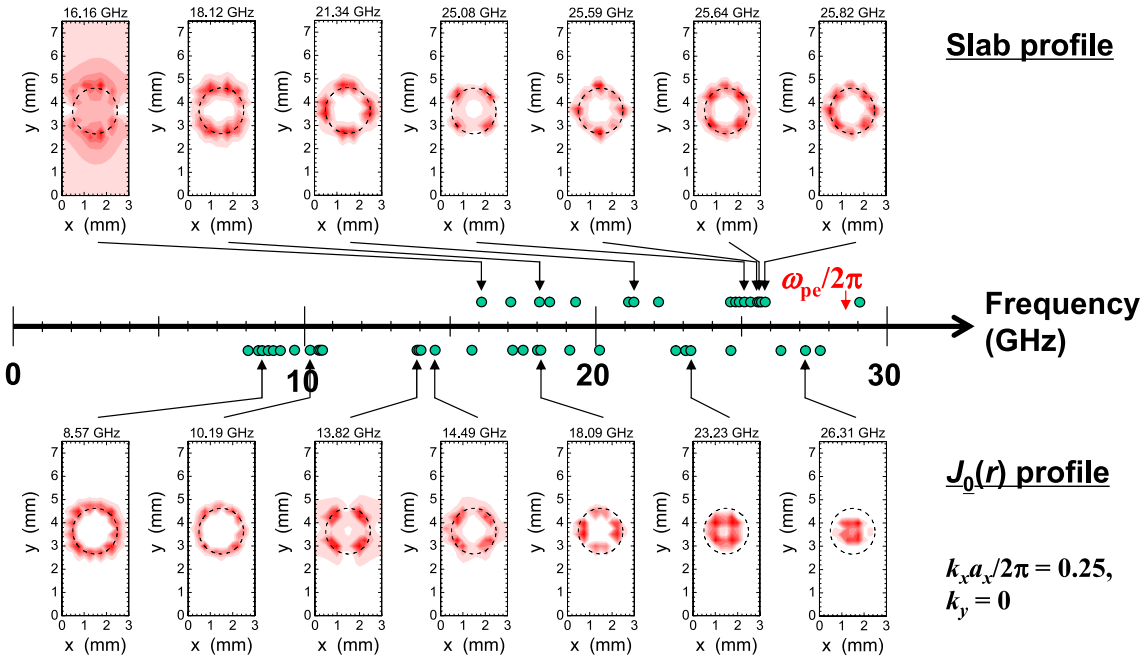

Fig. 5 Spatial profiles of wave electric fields in one rectangular lattice of a microplasma array with parameters similar to those in Fig. 4.

present at up to $\omega_{pe}/\sqrt{2}$; this is not consistent with the case in Fig. 5, because a microplasma in this configuration is not single but forms periodic structure that raises the upper frequency limit [12].

In the lower part of Fig. 5, profiles in the density-gradient case exhibit some features common to the slab case, but clearly different points are also found. Electric fields concentrated on the boundary of the microplasma column at low frequencies, which was similar to the profiles in the slab case. However, as the frequency increased, localized electric fields spread into the central region. Furthermore, the lower limit of the wave propagation was down to 8 GHz, which was approximately half that of the slab case. These features are due to radial dependence of ω_{pe}; because a density gradient exists in the plasma column and the characteristic length of its gradient exceeds the width of the localized electric-field profile, electric fields are present just outside the layer of "local" electron plasma frequency.

This shrinking of the localized electric-field area might give rise to change in the attenuation of transmitted waves. At higher frequencies near ω_{pe}, there exist propagating modes with electric fields inside a microplasma column, and their wave energy penetrates through its outer region. Collisional damping and accumulated attenuation of the waves along a microplasma chain would reduce transmission efficiency.

3. Experimental Results

3.1 Band gap in lossy photonic crystals

We briefly review experiments on lossy photonic crystals, which are described in detail in Ref. [14].

A columnar plasma was confined in a fine cold cathode fluorescent lamp (CCFL) tube, i.e., a glass tube with an outer diameter of 1.8 mm and thickness of 0.2 mm. The discharge gas was an Ar and Ne mixture with Hg evaporated from liquid mercury. A bipolar square-pulsed voltage was applied to the electrodes with an individual series resistance of 47 kΩ, and the pulse width was set to 5 μs with a repetition frequency of 30 kHz. The voltage amplitude was 1.5-2.2 kV as a zero-to-peak value. That is, this discharge was operated in a direct-current pulse mode. Experimental data for microwave transmission on microstrip and coplanar lines with an adjacent CCFL array indicated that the electron density in this columnar plasma was 0.4-1.0 × 10^{13} cm^{-3} [14], which corresponds to $\omega_{pe}/2\pi$ at 18-28 GHz. The CCFLs in this experiment demonstrated here were arranged between the conductors of a usual coplanar waveguide conductors with periodic length a = 3.0-12.0 mm.

Transmittance, defined as the ratio of a transmitted-wave power when plasmas were turned on to that when they were turned off, showed a decrease resembling that of k_i, as shown in Fig. 2. However, a reduction of wave attenuation was observed in a narrow band just below the first band gap predicted theoretically. This was attributed to wave-field profiles that change just below the band gap [12], as mentioned in Sec. 2.1; in Fig. 3, k_i decreases as the frequency increased, with a minimum value just below the band gap around $\omega a/2\pi c$ = 0.29 because the electric fields are less in the plasma region where the waves attenuate via elastic collisions. It then jumped up by one order of magnitude just above the band gap around $\omega a/2\pi c$ = 0.32. In the experimental observations, a band with such a huge k_i is similar to the state in the band gap

where wave propagation is forbidden. That is, this band-gap material works as a band-*pass* filter that has a pass band just below the band gap.

We point out, as a reference, the case of periodic lossless dielectrics such as photonic crystals in the photon range; $k_r(\omega)$ around the band gap is very similar to that shown in Fig. 3, and two frequency bands are present at the same $k_r(k_r a/2\pi = 0.5)$, so that the stored energy in the electromagnetic fields should differ in the two bands. Then, above the band gap, the electric fields are localized in the "air" where the permittivity is smaller, and below the band gap the electric fields are localized in the dielectric where the permittivity is larger. Inside the band gap region, the density of states is zero since their presence is forbidden, leading to a band-*stop* filter. That is, both the phenomenon in lossy plasma periodic structures similar to a band-pass filter and that in a lossless dielectric periodic structure similar to a band-stop filter arise from the frequency band gap, which gives rise to the change in the field profiles.

Another aspect of the measured frequency spectra of transmitted waves leads to diagnostics of plasma parameters through derivation of band diagrams by surveying parameters such as n_e and electron temperature T_e, which mainly affects k_r and k_i, respectively; T_e can be revealed by estimation of elastic collision frequency in the Drude model.

3.2 Dynamic waveguide of a microplasma chain

In this experiment, we also used similar CCFLs to construct a microplasma array, as described in Sec. 3.1. Here we arranged CCFLs to form a 1D array; a very simple "chain" structure.

To launch microwaves at one end of the chain and to detect them at the other end, truncated microstrip lines were set at both ends. A microwave generator (Agilent Technology, 83624B) swept frequencies from 2 to 20 GHz very slowly, in contrast to discharge voltage pulses at a 6.0-30 kHz repetition. Transmitted signals were detected by a rectifier diode and recorded in a digital storage oscilloscope.

Figure 6 shows transmittance as a function of microwave frequency. Here the definition of transmittance is similar to that in Sec. 3.1, so it indicates an enhancement factor due to plasma generation. The frequency spectrum of the transmittance shows a number of distinct and sharp peaks at 5-17 GHz; each mode of microwave propagation supported by the plasma chain was in a very narrow frequency region. Wwithout plasma generation, microwaves localized on the open edge of the microstrip line spread only in a near-field mode, which does not propagate as a far-field electromagnetic wave. That is, this enhancement of transmitted waves is attributed to wave propagation along the chain of these microplasma columns.

Figure 7 displays typical time evolutions of transmitted microwave signals with a discharge voltage signal. When microplasmas were not generated in CCFLs, detected signals came from the excitation of near fields on an open-ended microstrip line. When microplasmas were turned on, the transmitted signals were enhanced by a factor of 1-7, which indicates performance of a dynamic waveguide alive only during plasma generation. The rising phase of detected microwaves was during and just after the discharge voltage pulses, which indicates that plasma gen-

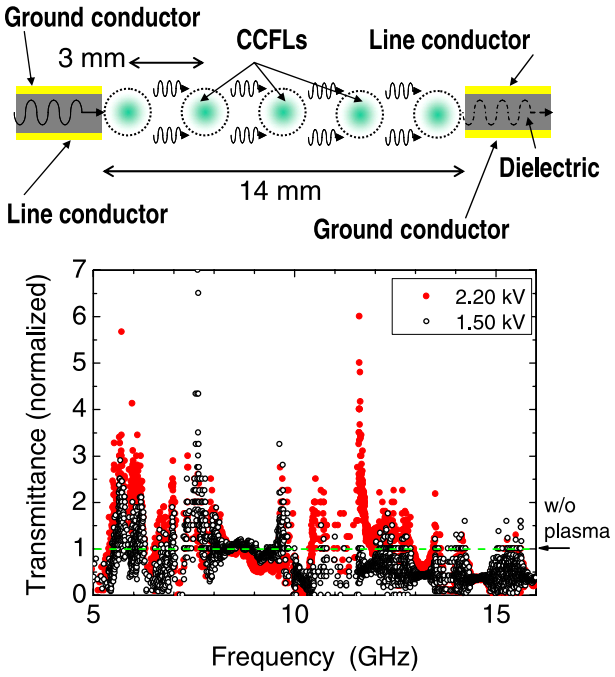

Fig. 6 Schematic view of experimental setup and transmittance spectra at 11 μs after discharge pulse. Bipolar voltage with 2.4-μs-wide square pulse is used. Time evolution of signals of transmitted waves is shown in Fig. 7.

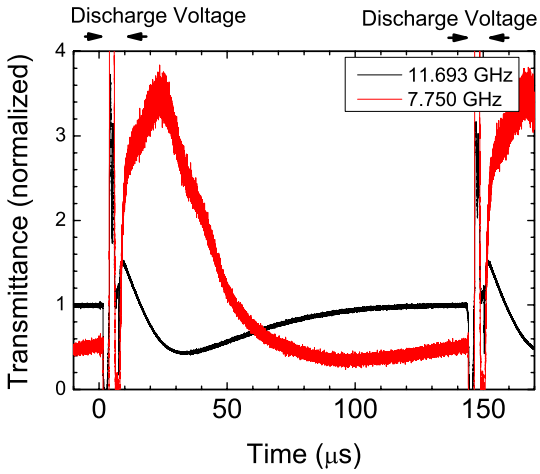

Fig. 7 Time evolutions of signals of transmitted waves at two wave frequencies. Experimental setup was similar to that in Fig. 6.

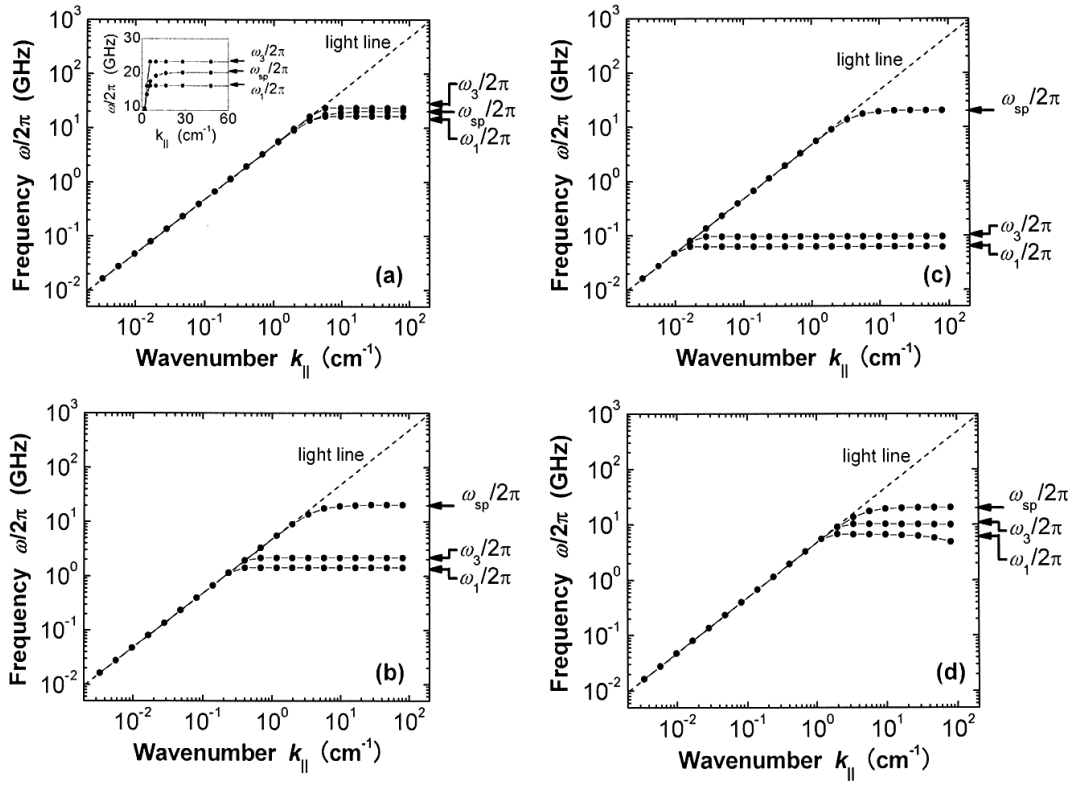

Fig. 8 Dispersion relation of surface waves on a layer with n_e-gradient profile. The maximum n_e is 1×10^{13} cm^{-3}. (a) $\alpha_1 = 3 \times 10^6$ cm^{-1}, (b) $\alpha_1 = 2 \times 10^4$ cm^{-1}, and (c) $\alpha_1 = 4 \times 10^1$ cm^{-1}. When we calculate the dispersion relation in (d), we assume a pressure term as $m_e\beta^2 n_e$, similar to the metal case, and $\alpha_1 = 4 \times 10^1$ cm^{-1}.

eration led to this signal enhancement. After the saturation of the enhanced signals, they attenuated gradually, but their attenuation rate and phase depend on wave frequency. This is partly because n_e changes in the afterglow phase after the discharge voltage is turn off; the condition of wave propagation on a flat band at each frequency varies one by one. Furthermore, because k_i is different in each flat band, the evolution of transmittance varies with time in a different manner.

Both experimental and numerical results strongly suggest that the observed microwave propagation arose from wave propagation on the LSP-like-mode chain. However, there might be other influences which would come from geometrical effects. In the experiment shown here, only five CCFLs were set, and finite array effects should be considered. This finite size might also yield reflection back and forth on each CCFL, which would lead to phenomena like Fabry-Perot interference. Such other effects will be discussed in the future, but in practical terms this microwave waveguide holds promise for forming a dynamic and flexible waveguide, independent of its physical mechanism.

4. Discussion

Figures 4, 5, and 6 indicate that surface waves were in a wider band than surface plasmon polaritons around a small metallic sphere for $\omega_{pe}/\sqrt{3} < \omega < \omega_{pe}/\sqrt{2}$; on a microplasma array, numerical results indicated that surface waves propagated at a much lower frequency than ω_{pe}, and transmittance enhancement, possibly by surface waves, was observed in the experiments. The numerical analysis shown in Sec. 3.2 was based on a plasma equivalent to a "cold" dielectric. Here we perform theoretical analysis based on the fluid model [20, 28–31], that is, a momentum balance equation including a term for electron pressure p_e.

The momentum balance equation of electrons in a gas discharge is described as

$$mn_e(z)\frac{d\boldsymbol{v}_e(z)}{dt} = -n_e(z)e\boldsymbol{E}(z) - \nabla p_e(z) - mn_e(z)\boldsymbol{v}_e(z)\nu_m, \quad (2)$$

where t is the time, $\boldsymbol{v}_e$ the electron fluid velocity, e the charge of an electron, and $\boldsymbol{E}$ the electric field. z is set along the gradient of n_e density profile. In metal optics, a similar description is referred to as the hydrodynamic formulation. Each variable is divided into static and fluctuating (wave-field) parts such as $n_e = n_{e0} + n_{e1}$, and the fluctuating part was considered to derive surface-mode dispersion relations, although the first term of the right-hand side in Eq. (2) is approximately replaced by $-n_{e0}(z)e\boldsymbol{E}_1 = \varepsilon_0 m\omega_{pe0}^2(z)\boldsymbol{E}_1$. Parker *et al.* pointed out [20] that, if we consider a "cold" dielectric which has only spatially con-

tinuous change in dielectric constant with a decrease of $n_{e0}(z)$ down to zero, the surface waves propagating along its surface have a *continuous* frequency spectrum down to much lower frequencies than ω_{pe}, as shown in Figs. 4 and 5.

However, a gas-discharge plasma with finite electron temperature is not the case, and we have to solve Eq. (2) with Poisson's equation, the continuity equation, and adequate boundary conditions [29]. When we assume that a plasma is in the state of 1D adiabatic compression, we can set $p_{e1}(z) = 3kT_e n_{e1}(z)$, where k is the Boltzmann constant. Following the previous analyses [28, 29], we assume $n_{e0}(z)$ profile of $\omega_{pe0}^2(z) = \omega_{pe0}^2(-\infty)(1 - \cosh^{-2}(\alpha_1 z))$, where α_1 represents the surface diffuseness of the $n_{e0}(z)$ profile, and $1/\alpha_1$ is approximately the width of the electron-density gradient region in the plasma edge. That is, α_1 directly affects the first term of the right-hand side of Eq. (2), and the derived dispersion relations are strongly deformed by α_1.

Figure 8 shows several cases of dispersion relations of surface wave modes derived from Eq. (2). Here we show the main mode saturating at $\omega_{sp} = \omega_{pe}/\sqrt{2}$, the first lowest mode at a resonance frequency ω_1, and the second lowest mode at a resonance frequency ω_3. When we reduce α_1 and make the density profile softer, the frequency spectra of the two lowest modes becomes by two orders of magnitude lower than ω_{sp}, as shown in Figs. 8 (a)-(c).

When we considered sheath formation on the plasma edge, the propagation mode at the very low frequencies in Fig. 8 (c) should be ruled out, since the boundary condition assumed in Ref. [29] in which polarization disappears at the edge might not be true; for instance, if we consider periphery plasma with n_e of 1×10^{12} cm^{-3}, the sheath thickness is tens of μm [32], which is one order of magnitude smaller than the plasma radius. As a result, the lowest frequency spectrum of the surface waves on a plasma in the experiment would be around 1 GHz. If we adopt a pressure term similar to that of metals, $p_{e1}(z) = m_e\beta^2 n_{e1}(z)$, where $\beta^2 = (3/5)v_F^2$ and v_F is the Fermi velocity [27], the frequency spectra of the two lowest modes remain in a range similar to that of ω_{sp}, as shown in Fig. 8 (d). That is, the wide band of surface wave modes on the microplasma array is attributed to a soft density gradient on the edge, except for the sheath region and the pressure term in the momentum balance.

In Secs. 2.1 and 2.2 we described two distinct but different features of a microplasma array at $\omega < \omega_{pe}$. Here we briefly discuss their emerging conditions. The band gap, which occurs around $n\omega a/(2\pi c) \sim 0.5$, where n is the refractive index, is clear when a has a range similar to that of the wavelength and a significant spatial gap exists between microplasmas. On the other hand, plasmon chains or flat bands in the dispersion relation are dominant when the spatial gap between microplasmas is relatively small in comparison with the wavelength and can be present at frequencies much less than ω_{pe} due to its large wavenumber. Parameters used in Figs. 1 and 4 meet such requirements for each case.

5. Summary

A microplasma array at frequencies less than ω_{pe} serves as a photonic crystal, which is a band-gap material equivalent to a band-pass filter, and as a plasmon chain, which becomes a dynamic waveguide. We drew a band diagram of a microplasma array in a 3D $\omega - k_r - k_i$ space, which clarified the band-gap properties including a frequency gap and attenuation discontinuity. Such features have not been noted in the previous reports of (metallic) photonic crystals. Plasmon chains composed of microplasma arrays functioned as a dynamic waveguide, and their frequency spectra were fairly wide. Such a feature of wave propagation mainly depends on soft n_e gradient on the edge. These microplasma array functions, verified in this report, will lead to novel wave controller devices from the microwave to the terahertz wave range.

Acknowledgments

This work was supported in part by Grants-in-Aide for Scientific Research from the Japanese Ministry of Education, Culture, Sports, Science, and Technology, and by the Industrial Technology Research Grant Program of 2006 from the New Energy and Industrial Technology Development Organization (NEDO) of Japan.

[1] T.H. Stix, *The Theory of Plasma Waves* (McGraw-Hill, New York, 1962).
[2] V.L. Ginzburg, *The Propagation of Electromagnetic Waves in Plasma* (Pergamon Press, Oxford, 1964).
[3] E. Yablonovitch, Science **289**, 557 (2000).
[4] S. Noda and T. Baba, ed., *Roadmap on Photonic Crystals* (Kluwer Academic Publishing, Boston, 2003).
[5] J. Faith, S.P. Kuo and J. Huang, Phys. Rev. E **55**, 1843 (1997).
[6] D.K. Kalluri, *Electromagnetics of Complex Media* (CRC Press, Boca Raton, 1998).
[7] H. Hojo and A. Mase, J. Plasma Fusion Res **80**, 89 (2004).
[8] O. Sakai, T. Sakaguchi and K. Tachibana, Appl. Phys. Lett. **87**, 241505 (2005).
[9] O. Sakai, T. Sakaguchi, Y. Ito and K. Tachibana, Plasma Phys. Control. Fusion **47**, B617 (2005).
[10] O. Sakai, T. Sakaguchi and K. Tachibana, J. Appl. Phys. **101**, 073304 (2007).
[11] T. Sakaguchi, O. Sakai and K. Tachibana, J. Appl. Phys. **101**, 073305 (2007).
[12] O. Sakai and K. Tachibana, IEEE Trans. Plasma Sci. **35**, 1267 (2007).
[13] O. Sakai, T. Sakaguchi, T. Naito, D.-S. Lee and K. Tachibana, Plasma Phys. Control. Fusion **49**, B453 (2007).
[14] T. Naito, O. Sakai and K. Tachibana, Appl. Phys. Express **1**, 066003 (2008).
[15] J.R. Krenn, A. Dereux, J.C. Weeber, E. Bourillot, Y. Lacroute, J.P. Goudonnet, G. Schider, W. Gotschy, A. Leitner and F.R. Aussenegg, Phys. Rev. Lett. **82**, 2590 (1999).
[16] M.L. Brongersma, J.W. Hartman and H.A. Atwater, Phys.

Rev. B **62**, R16356 (2000).
[17] S.A. Maier, P.G. Kik, H.A. Atwater, S. Meltzer, E. Harel, E., B.E. Koel and A.A. Requicha, Nature Mat. **2**, 229 (2003).
[18] A.W. Trivelpiece and R.W. Gould, J. Appl. Phys. **30**, 1784 (1959).
[19] J.C. Nickel, J.V. Parker and R.W. Gould, Phys. Rev. Lett. **11**, 183 (1963).
[20] J.V. Parker, J.C. Nickel and R.W. Gould, Phys. Fluids **7**, 1489 (1964).
[21] H.C. Hoh, Phys. Rev. **133**, A1016 (1964).
[22] D.J. Cooperberg, Phys. Plasmas **5**, 862 (1998).
[23] Y. Yasaka and H. Hojo, Phys. Plasmas **7**, 1601 (2000).
[24] I.P. Ganachev and H. Sugai, Surf. Coat. Technol. **200**, 792 (2005).
[25] K.C. Huang, E. Lidorikis, X. Jiang, J.D. Jannopoulos, K.A. Nelson, P. Bienstman and S. Fan, Phys. Rev. B **69**, 195111 (2004).
[26] T. Ito and K. Sakoda, Phys. Rev. B **64**, 045117 (2001).
[27] F. Forstmann and R.R. Gerhardts, *Metal Optics Near the Plasma Frequency* (Springer-Verlag, Berlin, 1986).
[28] A. Eguiluz and J.J. Quinn, Phys. Rev. B **14**, 1347 (1976).
[29] J.E. Sipe, Surf. Sci. **84**, 75 (1979).
[30] C. Schwartz and W.L. Schaich, Phys. Rev. B **26**, 7008 (1982).
[31] J.M. Pitarke, V.M. Silkin, E.V. Chulkov and P.M. Echenique, Rep. Prog. Phys. **70**, 1 (2007).
[32] M.A. Lieberman and A.J. Lichtenberg, *Principles of Plasma Discharges and Materials Processing* (John Wiley & Sons, New York, 1994).